Characteristics analysis of the senjo-kousuitai conditions in the Kyushu region in early July: The case of the July 2020 heavy rainfall event

Masaki Satoh[1], and Keisuke Hosotani[1]

[1]*Atmosphere and Ocean Research Institute, The University of Tokyo, Kashiwa, Japan*

Submitted to SOLA, 7 Oct. 2022

Special collection on "Research on extreme weather events that occurred around East Asia in 2017-2021"

Corresponding author: Masaki Satoh, Atmosphere and Ocean Research Institute, The University of Tokyo, 5-1-5 Kashiwanoha, Kashiwa, 277-8564, Japan. E-mail: satoh@aori.u-tokyo.ac.jp; tel: +81-4-7136-6050; fax: +81-4-7136-6056

Running title: Characterizing senjo-kousuitai conditions in the Kyushu region in early July

Abstract

A sequence of heavy rainfall events due to quasi-stationary band-shaped precipitation systems, or "senjo-kousuitai", was observed in the Kyushu region, Japan, from 3 to 8 July 2020. In this study, we investigate two of six indices that have previously been used to determine conditions favorable for senjo-kousuitai: water vapor flux at 500 m height and

helicity relative to the storm. We examine the relationship between these indices and the occurrence of senjo-kousuitai over the past 20 years. We show that the anomaly in wind speeds rather than humidity contributes more to anomalous water vapor flux. The vertical shear of zonal winds and the meridional flow in the lower layer contribute more to the storm-relative helicity. We conducted 20-member ensemble experiments with a 14 km mesh Nonhydrostatic Icosahedral Atmospheric Model (NICAM) for the senjo-kousuitai event with the initial condition at 0000 UTC on 3 July before the heavy rainfall event. We found that the initial variabilities of the water vapor over the area stretching from the East China Sea to the South China Sea and the wind fields over the western periphery of the North Pacific subtropical high are sensitive to the water vapor flux over the senjo-kousuitai area in Kyushu.

(Satoh, M. and K. Hosotani, 2022: Characteristics analysis of the senjo-kousuitai conditions in the Kyushu region in early July: The case of the July 2020 heavy rainfall event. *SOLA*, **XX**, XXX-XXX, doi:10.2151/sola.yyyy-nnn.)

1. Introduction

The July 2020 heavy rainfall event comprised torrential rain that occurred from 3 to 31 July 2020 across western to eastern Japan and the Tohoku region. In particular, the Kyushu region experienced record-breaking rainfall from 3 to 8 July that exceeded 120 mm h^{-1} and caused significant damage as a result of major rivers overflowing. Over these five days and nine cases of quasi-stationary band-shaped precipitation systems, or “senjo-kousuitai”, that is, areas of stagnant, intense rainfall with a quasi-linear distribution, were

identified in the Kyushu region, the highest number recorded since 2009 (Hirockawa et al. 2020). The spatial and temporal scales of each senjo-kousuitai were about 270 km and 10 h, respectively. In particular, the senjo-kousuitai that stagnated near the Kuma River from 3 to 4 July had a stagnation time of 13 h, the longest duration recorded since 2009 (Hirockawa et al. 2020).

Characteristics of the atmospheric environmental conditions during the July 2020 heavy rainfall event have been studied by Hirockawa et al. (2020), Araki et al. (2021), and Tochimoto et al. (2022). The predictability of this heavy rainfall event was investigated by Duc et al. (2021), Maejima et al. (2022), and Terasaki and Miyoshi (2022) using ensemble simulations and by Ikuta et al. (2022) in terms of how it is affected by the ship observation. Terasaki and Miyoshi (2022) demonstrated that 1024 ensemble members effectively show a spatial pattern of lag correlation between heavy rainfall and the precursors of the meteorological condition. Zhao et al. (2021) analyzed the root of the moisture transport to the heavy rainfall regions.

In Kato (2020), a statistical analysis shows six environmental conditions that characterize heavy rainfall due to senjo-kousuitai. Of these, water vapor flux (FLWV) at 500 m altitude and storm-relative helicity (SREH) are the two conditions most distinctly related to the intense rainfall attributed to senjo-kousuitai (Goto and Satoh 2022). Therefore, this study focuses on the FLWV and SREH of the July 2020 heavy rainfall event. We analyzed these indices at the time of occurrence and compared them with the condition in the Kyushu region in early July over the past 20 years.

We also conducted ensemble numerical experiments for a heavy rainfall event in early July 2020 to show which areas of the water vapor and wind fields of the initial condition are sensitive to the water vapor flux over the area of the heavy rainfall event.

We discuss our analyses of FLWV and SREH in Section 2 and show the results of the ensemble numerical experiments in Section 3. Concluding remarks are presented in Section 4.

2. Environmental conditions in early July in the Kyushu region

We analyzed the environmental fields in early July over the 20 years from 2001 to 2020 to identify the characteristics of the senjo-kousuitai indices in 2020. We mean early July by the period between July 1 and 10. Heavy rainfalls were frequently observed over the Kyushu region in early July; 2005, 2007, 2014, 2017, 2018, and 2020 are the years when heavy rainfall caused disasters in the Kyushu region [Japan Meteorological Agency, https://www.data.jma.go.jp/obd/stats/data/bosai/report/index_1989.html (in Japanese; accessed on 7 Oct. 2022)]. Among the six conditions favorable for senjo-kousuitai (Kato 2020), we focused on FLWV and SREH because they are distinctive between heavy rainfall events attributed to senjo-kousuitai and those not attributed to senjo-kousuitai (Goto and Satoh 2022). We use the JMA 55-year reanalysis data (Kobayashi et al. 2015).

FLWV was calculated using the air density ρ, mixing ratio of water vapor q, and wind speed v as

$$\mathrm{FLWV} = \rho q v. \tag{1}$$

These values were evaluated at an altitude of 500 m above sea level (a. s. l.) for the surface height below 300 m a. s. l.; for a surface height above 300 m a. s. l., the values were evaluated at 200 m above ground level. Unless otherwise indicated, the values at 500 m a. s. l. were used as the index.

SREH is defined as

$$\mathrm{SREH} = \int_{0\mathrm{km}}^{3\mathrm{km}} (\boldsymbol{v} - \boldsymbol{c}) \cdot \boldsymbol{\omega} dz, \quad (2)$$

where $\boldsymbol{v}$ is horizontal wind velocity, $\boldsymbol{c}$ is the traveling vector of the storm, and $\boldsymbol{\omega}$ is horizontal vorticity associated with vertical shear. Following Kato (2020), we defined $\boldsymbol{c}$ as the density-weighted average of the wind between 0 and 6 km, rotated clockwise by 30° and multiplied by 0.75, as originally proposed by Maddox (1976).

Figure 1a, 1c shows the horizontal distributions of FLWV and SREH at 1800 UTC on 3 July over the area covering western Japan, the East China Sea, the western North Pacific, and China, together with the anomalies of these values relative to the climatology (Fig. 1b, d). In the ocean area extending from the East China Sea to the southwest of Japan, the values of the six senjo-kousuitai indices frequently meet the conditions necessary for senjo-kousuitai (Goto and Satoh 2022). In the case of FLWV and SREH, the conditions that favor the occurrence of senjo-kousuitai are FLWV > 150 g m^{-2} s^{-1} and SREH > 100 m^{-2} s^{-2} (Kato 2020). Both FLWV and SREH values meet these conditions along the south coast of western Japan and in the southern area of the East China Sea. In this case, a zone of abundant column-integrated water vapor (precipitable water) extends from western Japan to China (Fig. 2). It corresponds closely to the zones of the anomalous values of FLWV and SREH (Fig. 1b, 1d). Figure 1a, 1b also shows wind vector $\boldsymbol{v}$ and water vapor mixing ratio q at an altitude of 500 m. The anomalies of FLWV and these quantities relative to the climatological values over the period spanning 1–10 July are also shown (Fig. 1b). In this period, FLWV is higher than the climatology along the zonal area from western Japan to the south of China. Figure 1b indicates that not only the anomaly of q

but also that of wind speed v contributes to the anomaly of FLWV.

To quantify the relative importance of q and v for FLWV, we analyzed the interannual variation of FLWV in early July (1–10 July) from 2001 to 2020 over the Kyushu region. The average value over 20 years is denoted by $\bar{}$ and is referred to as the climatology. The deviation from the climatology is denoted by $'$. For the analysis of FLWV, we neglected variations of ρ and investigated the contribution of q and v; the contributions to FLWV by each term of $(qv)' = \bar{q}v' + q'\bar{v} + q'v'$ are shown in Fig. 3. Over the 20-year period of interest, heavy rainfall events in Kyushu in early July were reported in 2005, 2007, 2014, 2017, 2018, and 2020. In these years, the contribution of the positive deviation of wind speed $\bar{q}v'$ was larger than that of the mixing ratio $q'\bar{v}$, indicating a stronger contribution from wind speed. Our results for these years establish the predominant contribution of wind speed anomalies.

For the analysis of SREH, we first separated equation (2) into the contributions of zonal and meridional winds by using $\boldsymbol{v} = (u, v)$, $\boldsymbol{c} = (c_u, c_v)$, and $\boldsymbol{\omega} = (\omega_u, \omega_v)$ as

$$\text{SREH} = \int_{0\text{km}}^{3\text{km}} (u - c_u) \cdot \omega_u dz + \int_{0\text{km}}^{3\text{km}} (v - c_v) \cdot \omega_v dz, \tag{3}$$

Figure 4a shows vertical profiles of $u - c_u$, $v - c_v$, ω_u, and ω_v, and Fig. 4b shows those of $(u - c_u) \cdot \omega_u$ and $(v - c_v) \cdot \omega_v$. The profiles for 2020 (solid curves) are compared with those of the climatology (dashed curves). In 2020, the zonal shear and the meridional velocity are larger than the climatology. The anomalously stronger meridional velocity was already shown in Fig. 1b at 500 m a. s. l. Because ω_v is determined by the vertical shear of the zonal wind, ω_v is larger than the climatology. Therefore, as shown in Fig. 4b, $(v - c_v) \cdot \omega_v$ is larger than the climatology over all levels between 0 and 3

km. As also shown in Fig. 4b, the contribution of the second term on the right-hand side of equation (3) is larger than that of the first term. However, at levels below 1 km, the contribution of the first term becomes large mainly because of ω_u, the vertical shear of meridional velocity. The vertical shear of the zonal wind is associated with the larger-than-normal temperature gradient in the north-south direction in the Kyushu region. In rainy years, heavy rainfall is generally along the Baiu front. Figure 4 indicates that the stronger meridional wind with its lower-level vertical shear and the vertical shear of the zonal wind contributed significantly to the larger anomaly of SREH in early July of 2020.

We then found the contribution of each layer, 0–1 km, 1–2 km, and 2–3 km, to equation (2):

$$\mathrm{SREH} = \int_{0\mathrm{km}}^{1\mathrm{km}} (\boldsymbol{v}-\boldsymbol{c})\cdot\boldsymbol{\omega}dz + \int_{1\mathrm{km}}^{2\mathrm{km}} (\boldsymbol{v}-\boldsymbol{c})\cdot\boldsymbol{\omega}dz + \int_{2\mathrm{km}}^{3\mathrm{km}} (\boldsymbol{v}-\boldsymbol{c})\cdot\boldsymbol{\omega}dz, \quad (4)$$

Figure 5 shows the interannual variation in these contributions to SREH in early July from 2001 to 2020 in the Kyushu region. Almost every year, not just in the years with heavy rainfall (2005, 2007, 2014, 2017, 2018, 2020), the lowest layer, 0–1 km, makes the greatest contribution. Figure 5 shows that the lower-level shear and winds largely contribute to the anomalous SREH.

We further analyzed the relative contributions of anomalous wind components and vorticities. Here, we define storm-relative wind components $U = u - c_u$ and $V = v - c_v$, then we expand equation (2) as

$$\begin{aligned}\mathrm{SREH} &= \int_{0\mathrm{km}}^{3\mathrm{km}} (U\omega_u + V\omega_v)dz \\ &= \overline{\mathrm{SREH}} + \int_{0\mathrm{km}}^{3\mathrm{km}} (\bar{U}\omega_u' + U'\overline{\omega_u} + U'\omega_u' + \bar{V}\omega_v' + V'\overline{\omega_v} + V'\omega_v')dz. \end{aligned} \quad (5)$$

Figure 6 shows the year-to-year variation in each term of the second term on the right-hand side of equation (5) for the contributions of each layer 0–1 km, 1–2 km, and 2–3 km. Which term contributes the most varies from year to year, but generally, the terms $\bar{V}\omega_v'$, $V'\overline{\omega_v}$, and $V'\omega_v'$ in the 0–1 km layer make the greatest contribution. Therefore, in the Kyushu region, the variation in SREH values is related to the relative components of the southerly winds and the vertical shear of the zonal winds in the 0–1 km layer.

In 2020, the increase in the vertical shear of the lower-level zonal winds contributed to the increase in SREH. The contributions of $\bar{U}\omega_u'$, $U'\overline{\omega_u}$, and $U'\omega_u'$ were very large in 2018 and non-negligible in 2020 (Fig. 6a). The vertical shear of the zonal winds is related to the meridional temperature gradient. As shown in Fig. S1, the meridional temperature gradient on the 1000-hPa surface is larger than the climatology in the area along the Biau front from Kyushu to mainland China. The larger meridional temperature gradient area almost matches the more precipitable water area, as shown in Fig. 2.

3. Ensemble simulation with NICAM

The enhancement of the water vapor flux is key to heavy rainfall in the Kyushu region. The origin of the water vapor was traced back to the oceanic area southwest of Kyushu rather than to the western area in mainland China along the band of rich precipitable water (Fig. 2). To show which areas are more related to the rainfall over the Kyushu region, we performed ensemble experiments using the nonhydrostatic icosahedral atmospheric model (NICAM; Tomita and Satoh 2004; Satoh et al. 2008, 2014). We use 20 members of the NEXRA (NICAM-LETKF JAXA Research Analysis; https://www.eorc.jaxa.jp/theme/NEXRA/; Chen et al. 2022, manuscript in preparation) product at 00:00 UTC on 3 July 2020 as initial values. The horizontal grid interval of

NICAM is approximately 14 km, and 40 vertical levels are used up to the top of the model domain at an altitude of 40 km.

Figure 7a shows the spatial distribution of the correlation coefficient between the water vapor mixing ratio at 500 m a. s. l. at 00:00 UTC on 3 July and the rainfall in the Kyushu region (defined as the area [30-32.5°N, 130-133.75°E]) at 18:00 UTC on 3 July, which is the time of the heaviest rainfall in Kyushu between 3 and 8 July. We can see a positive correlation in the region extending from the East China Sea southwest of Kyushu to the South China Sea via the Taiwan Strait; in Fig. 7a, the thicker red and blue areas are significant for a correlation coefficient higher than 0.4 based on the *t*-test with a significance level of 0.05 for 20 members.

Figure 7b also shows the correlation coefficient between wind speed at 500 m a. s. l. at 00:00 UTC on 3 July and precipitation in Kyushu at 18:00 UTC on 3 July. Here, a positive correlation is seen in the area around the edge of the Pacific High. The surface pressure and its anomaly to the climatology between 1 and 10 July are shown in Fig. S2. A significant positive correlation (larger than 0.4) is situated between the 1010 and 1012 hPa contours of Fig. S2a. The east region of these areas has anomalously high pressure compared to the climatology (Fig. S2b).

The results of our ensemble experiments indicate that surface winds were enhanced along the periphery of the anomalously high pressure south of Japan. These winds transported more abundant water vapor from the southwest of Kyushu to the Kyushu region.

4. Conclusion

Our analysis suggests that the increase in water vapor flux (FLWV) at 500 m altitude and storm-relative helicity (SREH) in the July 2020 heavy rainfall event was influenced by enhanced south to south-westerly winds due to the southwest extension of the anticyclone, enhanced southerly winds relative to the rainfall area, and an increased north-south temperature gradient near the rainy season front.

We have analyzed the environmental conditions in the July 2020 heavy rainfall event with respect to FLWV and SREH at 500 m a. s. l.; two of six indices have been used to determine the favorable conditions for the occurrence of senjo-kousuitai. The factors that caused the increase in each index are summarized as follows.

We found that the FLWV value was influenced more by wind speed anomalies than by the water vapor content (Fig. 3). In particular, in 2020, the amount of water vapor near Kyushu was lower than normal. Still, the wind speeds were greater than normal, resulting in an above-normal FLWV. The results of the NICAM ensemble experiments indicate that in this heavy rainfall event, water vapor was brought to Kyushu from the area extending from the South China Sea to the East China Sea and the Pacific Ocean by the flows around the periphery of the Pacific High. This result is consistent with Zhao et al. (2021). The south-to-southwesterly winds were enhanced due to the southwesterly extension of the Pacific High.

For the SREH, the southerly component of storm-relative winds and the vertical shear of zonal winds contributed more in each layer below an altitude of 3 km, based on the vertical profiles of the average velocity and vorticity over Kyushu (Fig. 4). Furthermore, westerly wind speeds were also greater in the lower layers, with the largest

contribution to SREH due to the 0–1 km layer (Fig. 5). The larger vertical shear in the zonal winds was due to the larger than normal temperature gradient in the north-south direction (Fig. S1). The contribution of the 0–1 km layer to SREH was the largest throughout the 20 years. The main contributors to SREH are the southerly component of the storm-relative winds in the lower layers and the vertical shear of the zonal winds (Fig. 6). These results indicate that the north-south component of the lower-level storm-relative winds and the vertical shear of the zonal wind have a particularly large influence on SREH. In 2020, both of these components were larger than normal, contributing to the increase in SREH.

The above analysis elucidates the general properties of FLWV and SREH and could be used to investigate past and future cases. In addition, an analysis of the remaining four indices favorable for the occurrence of senjo-kousuitai would further deepen our understanding of the environmental conditions that cause senjo-kousuitai.

Supplements

Fig. S1: Horizontal distribution of anomaly of the meridional temperature gradient [K 2.5°] on the 1000-hPa surface in 2020 from the 20-year average.

Fig. S2: Horizontal distribution of (a) the surface pressure [hPa] averaged over the period between 1 and 10 July 2020 and (b) its anomaly from the 20-year average in the same period.

Acknowledgments

This work was supported by the Japan Society for the Promotion of Science, KAKENHI, Grant-in-Aid for Scientific Research B (20H01967) for Ultra Site for Measuring Atmosphere of Tokyo Metropolitan Environment and Collaboration Studies with High-Resolution Atmospheric Models (ULTIMATE). This work was also supported by MEXT (JPMXP1020200305) under the "Program for Promoting Researches on the Supercomputer Fugaku" (Large Ensemble Atmospheric and Environmental Prediction for Disaster Prevention and Mitigation).

Declaration

The authors have no conflicts of interest to declare.

Author contributions

M. S. and K. H. designed this study. K. H. analyzed the data and conducted numerical experiments of this study. M. S. and wrote the manuscript. M.S. and K.H. edited and approved the manuscript.

Data Availability Statement

The numerical experimental data are provided by requests to the authors.

Keywords

senjo-kousuitai, water vapor flux, storm-relative helicity, western North Pacific high

References

Araki, K., Kato, T., Hirockawa, Y., and Mashiko, W., 2021: Characteristics of atmospheric environments of Quasi-Stationary Convective Bands in Kyushu, Japan during the July 2020 Heavy Rainfall Event. SOLA 17, 8–15. doi:10.2151/sola.2021-002.

Duc, L., Kawabata, T., Saito, K., and Oizumi, T., 2021: Forecasts of the July 2020 Kyushu Heavy Rain using a 1000-member ensemble Kalman filter. SOLA 17, 41–47. doi:10.2151/sola.2021-007.

Goto, Y., and Satoh, M., 2022: Statistical Analysis of "Senjo-Kousuitai" in East Asia and Characteristics of Associated Large-scale Circulations in the Baiu season. SOLA, 18A, 15-20, https://doi.org/10.2151/sola.18A-003.

Hirockawa, Y., Kato, T., Araki, K., Mashiko, W., 2020: Characteristics of an extreme rainfall event in Kyushu district, southwestern Japan in early July 2020. SOLA, 16, 265-270.

Ikuta, Y., Seko, H., and Shoji, Y., 2022: Assimilation of shipborne precipitable water vapour by Global Navigation Satellite Systems for extreme precipitation events. Q. J. R. Meteorol. Soc. 148, 57–75. doi:https://doi.org/10.1002/qj.4192.

Kato, T., 2020: Quasi-stationary band-shaped precipitation systems, named "senjo-kousuitai", causing localized heavy rainfall in Japan. J. Meteor. Soc. Japan, 98,

485−509.

Kobayashi, S., Y. Ota, Y. Harada, A. Ebita, M. Moriya, H. Onoda, K. Onogi, H. Kamahori, C. Kobayashi, H. Endo, K. Miyaoka, and K. Takahashi, 2015: The JRA-55 Reanalysis: General specifications and basic characteristics. J. Meteor. Soc. Japan, 93, 5-48, doi:10.2151/jmsj.2015-001.

Maddox, R. A., 1976: An Evaluation of Tornado Proximity Wind and Stability Data. Mon. Wea. Rev., 104, 133-142.

Maejima, Y., Kawabata, T., Seko, H., and Miyoshi, T., 2022: Observing System Simulation Experiments of a Rich Phased Array Weather Radar Network Covering Kyushu for the July 2020 Heavy Rainfall Event. SOLA 18, 25–32. doi:10.2151/sola.2022-005.

Satoh, M., Matsuno, T., Tomita, H., Miura, H., Nasuno, T., Iga, S., 2008: Nonhydrostatic Icosahedral Atmospheric Model (NICAM) for global cloud resolving simulations. J. Comp. Phys., 227, 3486-3514, doi:10.1016/j.jcp.2007.02.006.

Satoh, M., Tomita, H., Yashiro, H., Miura, H., Kodama, C., Seiki, T., Noda, A. T., Yamada, Y., Goto, D., Sawada, M., Miyoshi, T., Niwa, Y., Hara, M., Ohno, Y., Iga, S., Arakawa, T., Inoue, T., Kubokawa, H., 2014: The Non-hydrostatic Icosahedral Atmospheric Model: Description and development. Prog. Earth Planet. Sci., 1, 18. doi:10.1186/s40645-014-0018-1.

Terasaki, K., and Miyoshi, T., 2022: A 1024-Member NICAM-LETKF Experiment for the July 2020 Heavy Rainfall Event. SOLA 18A, 8–14. doi:10.2151/sola.18A-002.

Tochimoto, E., Iizuka, S., and Ohigashi, T., 2022: Influence of an Upper-level Trough on the Formation of a Baiu Frontal Depression that Caused a Torrential Rainfall

Event in Southern Kyushu, Japan on July 4, 2020. SOLA 18A, 1–7. doi:10.2151/sola.18A-001.

Tomita, H. and Satoh, M., 2004: A new dynamical framework of nonhydrostatic global model using the icosahedral grid. Fluid Dyn. Res., 34, 357-400.

Zhao, N., Manda, A., Guo, X., Kikuchi, K., Nasuno, T., Nakano, M., Y. Zhang, and B. Wang, 2021: A Lagrangian view of moisture transport related to the heavy rainfall of July 2020 in Japan: Importance of the moistening over the subtropical regions. *Geophysical Research Letters*, 48, e2020GL091441. https://doi.org/10.1029/2020GL091441

List of Figure Captions

Fig. 1. Horizontal distributions of the indices related to senjo-kousuitai. (a) Water vapor flux (FLWV) [g m^{-2} s^{-1}] at 500 m altitude (colors), water vapor (contours) [g kg^{-1}], and wind vectors (arrows) [m s^{-1}] at 18:00 UTC on 3 July 2020. (b) The anomaly of the SREH average for 1–10 July 2020 relative to the 20-year average for the same period, the anomaly of water vapor (contours), and the anomaly of wind vectors (arrows). (c) Storm-relative helicity (SREH) [m^2 s^{-2}] at 18:00 UTC on 3 July 2020. (d) The anomaly of the SREH average for 1–10 July 2020 relative to the 20-year average for the same period.

Fig. 2. Horizontal distribution of precipitable water [kg m^{-2}] at 18:00 UTC on 3 July 2020.

Fig. 3: The 20-year variation in the contribution to the anomaly of water vapor flux

(FLWV) by neglecting variations in density, $(qv)' = \bar{q}v' + q'\bar{v} + q'v'$ [10^{-3} m s^{-1}], from 2001 to 2020.

Fig. 4: Vertical profiles of the contributions to storm-relative helicity (SREH). (a) Storm-relative velocity [m s^{-1}], $u - c_u$ (red), $v - c_v$ (blue), and vertical profiles of vorticity [s^{-1}], ω_u (green), and ω_v (magenta). Solid lines are for 2020, and dashed lines are for the 20-year average. (b) Components of the product of storm-relative velocity and vorticity [m s^{-2}], $(u - c_u) \cdot \omega_u$ (red) and $(v - c_v) \cdot \omega_v$ (blue).

Fig.5: The 20-year variation in the contribution of the 0–1 km (green), 1–2 km (blue), and 2–3 km (orange) layers of SREH [m^2 s^{-2}] to the total SREH [m^2 s^{-2}] (purple) for the years 2001 to 2020.

Fig. 6: The same as Fig. 5 but for each component of SREH. (a) $\bar{U}\omega_u'$, (b) $U'\overline{\omega_u}$, (c) $U'\omega_u'$, (d) $\bar{V}\omega_v'$, (e) $V'\overline{\omega_v}$, and (f) $V'\omega_v'$ [m s^{-2}].

Fig. 7: Horizontal distributions of the correlation between (a) precipitation rate at 18:00 UTC on 3 July and water vapor at 00:00 UTC on 3 July and (b) precipitation rate at 18:00 UTC on 3 July and wind speed at 00:00 UTC on 3 July.

Fig. S1: Horizontal distribution of the anomaly of the meridional temperature gradient [K 2.5°] on the 1000-hPa surface in 2020 relative to the 20-year average.

Fig. S2: Horizontal distribution of (a) the sea level pressure [hPa] averaged over the period from 1 to 10 July 2020 and (b) its anomaly relative to the 20-year average over the same period.

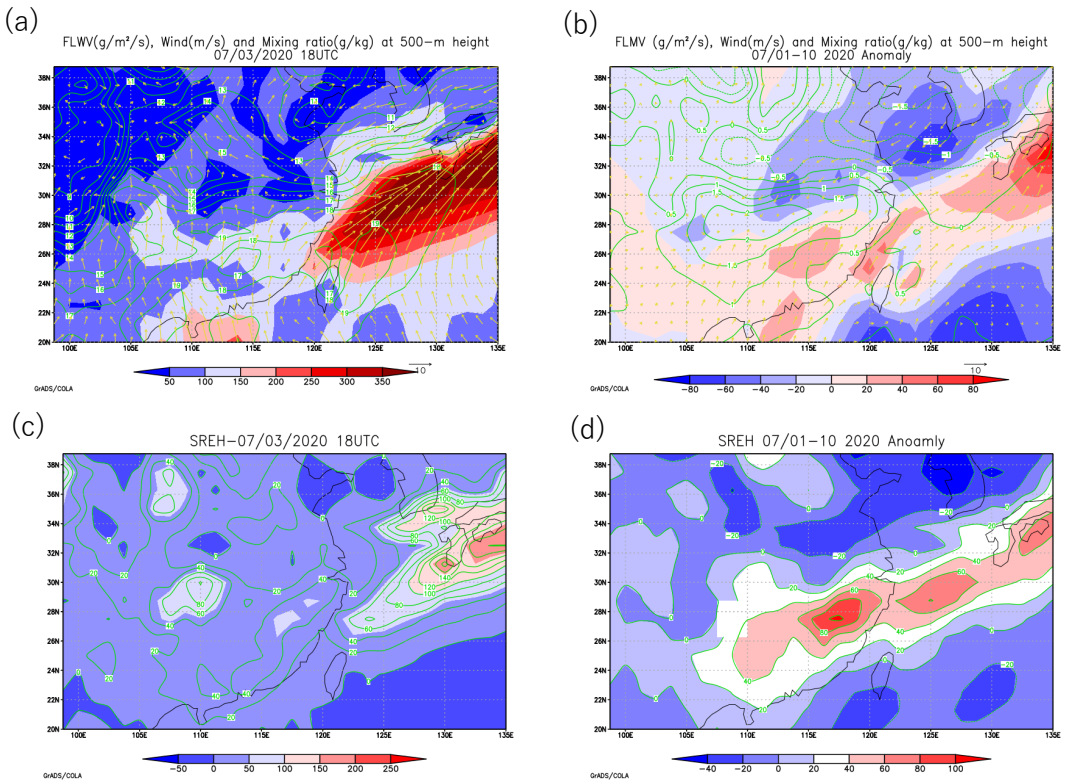

Fig. 1. Horizontal distributions of the indices related to senjo-kousuitai. (a) Water vapor flux (FLWV) [g m^{-2} s^{-1}] at 500 m altitude (colors), water vapor (contours) [g kg^{-1}], and wind vectors (arrows) [m s^{-1}] at 18:00 UTC on 3 July 2020. (b) The anomaly of the SREH average for 1–10 July 2020 relative to the 20-year average for the same period, the anomaly of water vapor (contours), and the anomaly of wind vectors (arrows). (c) Storm-relative helicity (SREH) [m^2 s^{-2}] at 18:00 UTC on 3 July 2020. (d) The anomaly of the SREH average for 1–10 July 2020 relative to the 20-year average for the same period.

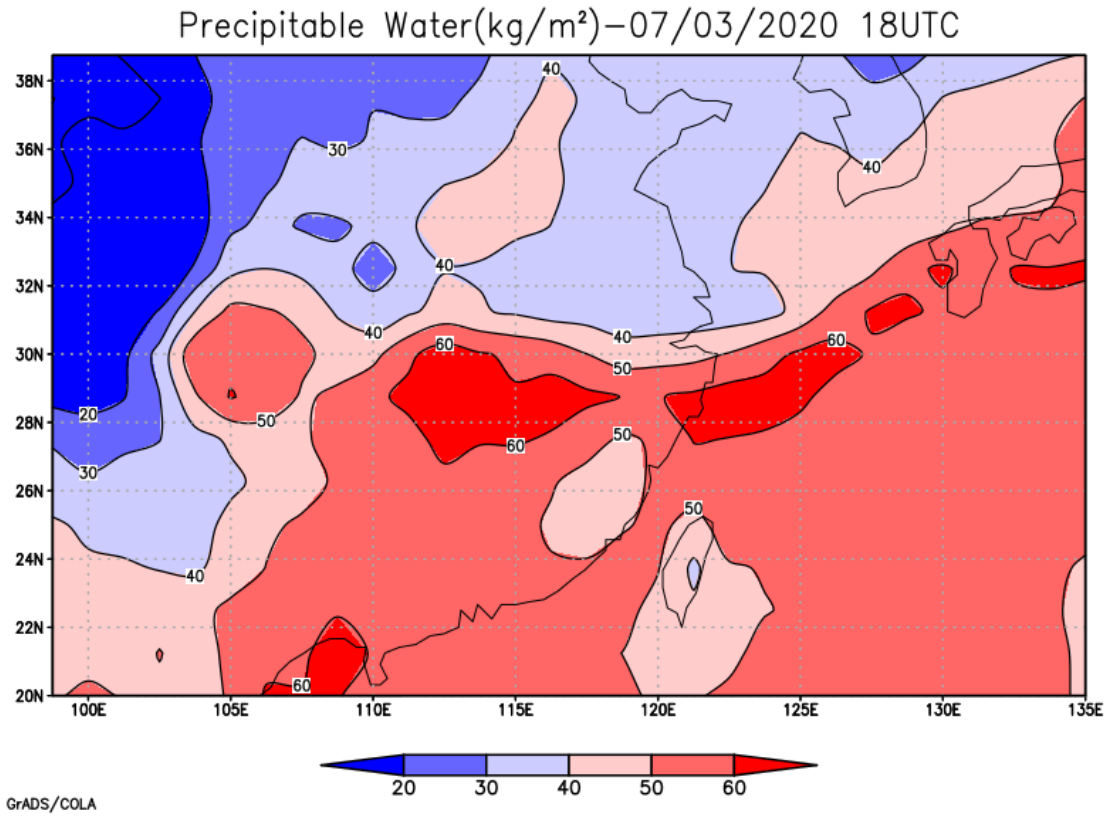

Fig. 2. Horizontal distribution of precipitable water [kg m^{-2}] at 18:00 UTC on 3 July 2020.

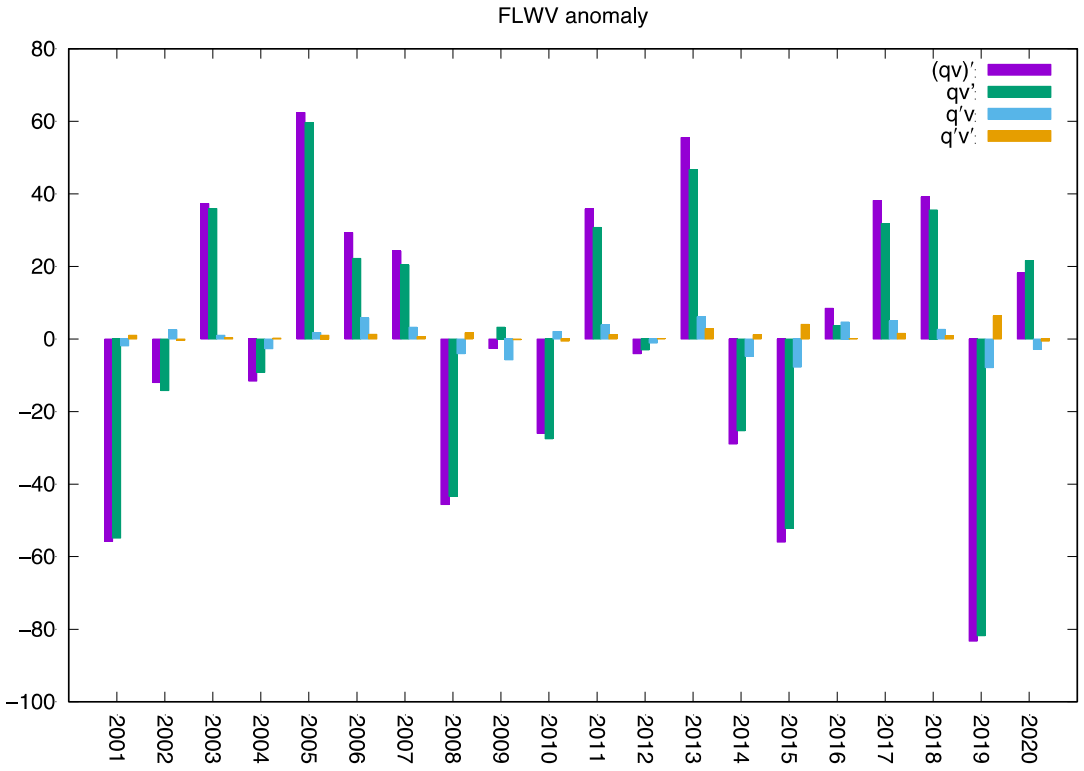

Fig. 3: The 20-year variation in the contribution to the anomaly of water vapor flux (FLWV) by neglecting variations in density, $(qv)' = \bar{q}v' + q'\bar{v} + q'v'$ [10^{-3} m s^{-1}], from 2001 to 2020.

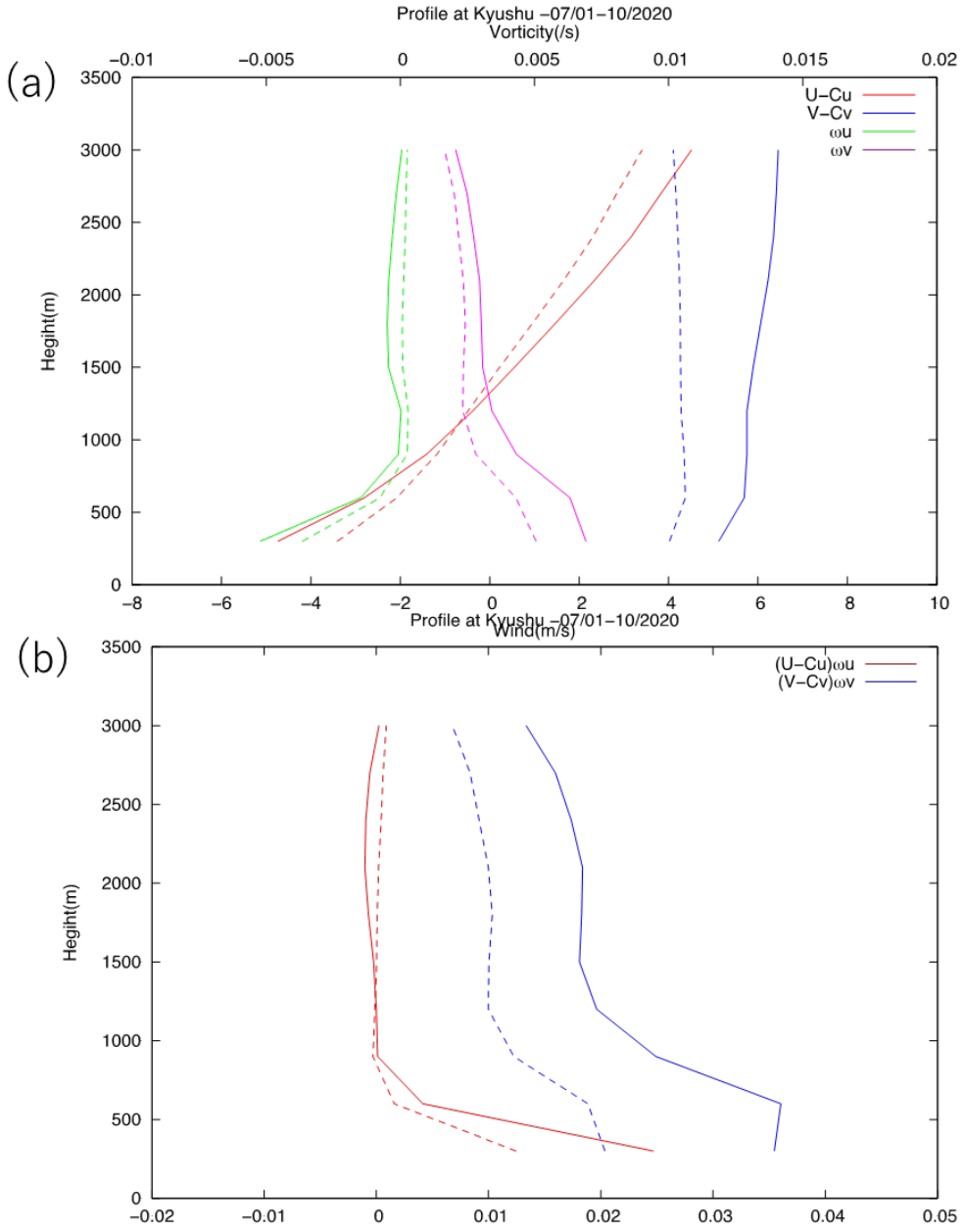

Fig. 4: Vertical profiles of the contributions to storm-relative helicity (SREH). (a) Storm-relative velocity [m s^{-1}], $u - c_u$ (red), $v - c_v$ (blue), and vertical profiles of vorticity [s^{-1}], ω_u (green), and ω_v (magenta). Solid lines are for 2020, and dashed lines are for the 20-year average. (b) Components of the product of storm-relative velocity and vorticity [m s^{-2}], $(u - c_u) \cdot \omega_u$ (red) and $(v - c_v) \cdot \omega_v$ (blue).

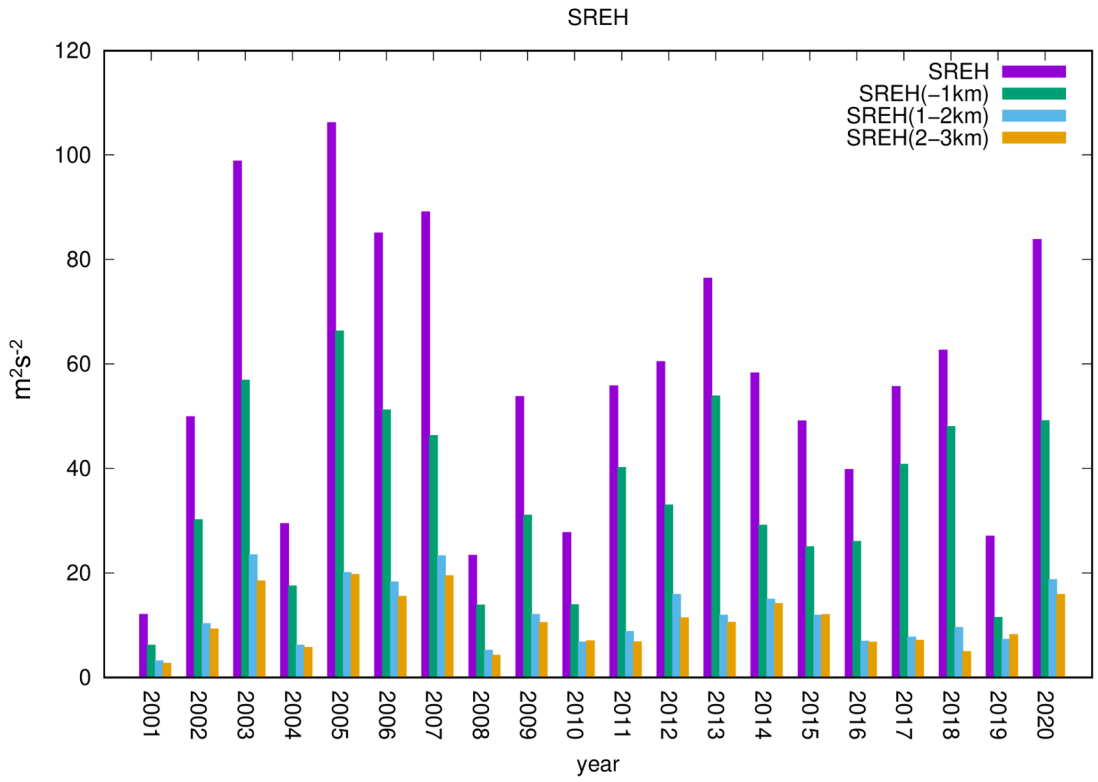

Fig.5: The 20-year variation in the contribution of the 0–1 km (green), 1–2 km (blue), and 2–3 km (orange) layers of SREH [m^2 s^{-2}] to the total SREH [m^2 s^{-2}] (purple) for the years 2001 to 2020.

1

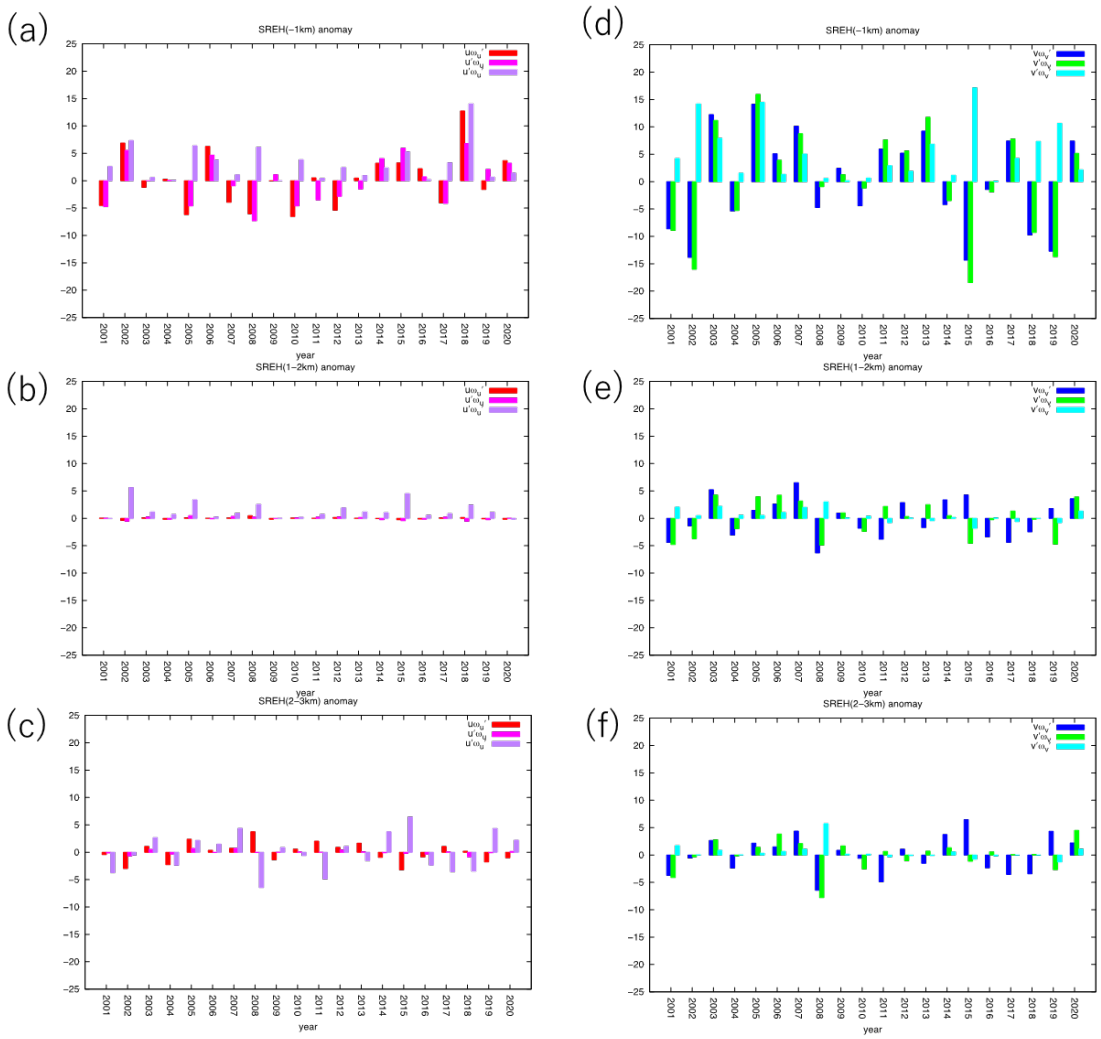

2

3 Fig. 6: The same as Fig. 5 but for each component of SREH. (a) $\bar{U}\omega_u'$, (b) $U'\overline{\omega_u}$, (c)

4 $U'\omega_u'$, (d) $\bar{V}\omega_v'$, (e) $V'\overline{\omega_v}$, and (f) $V'\omega_v'$ [m s^{-2}].

5

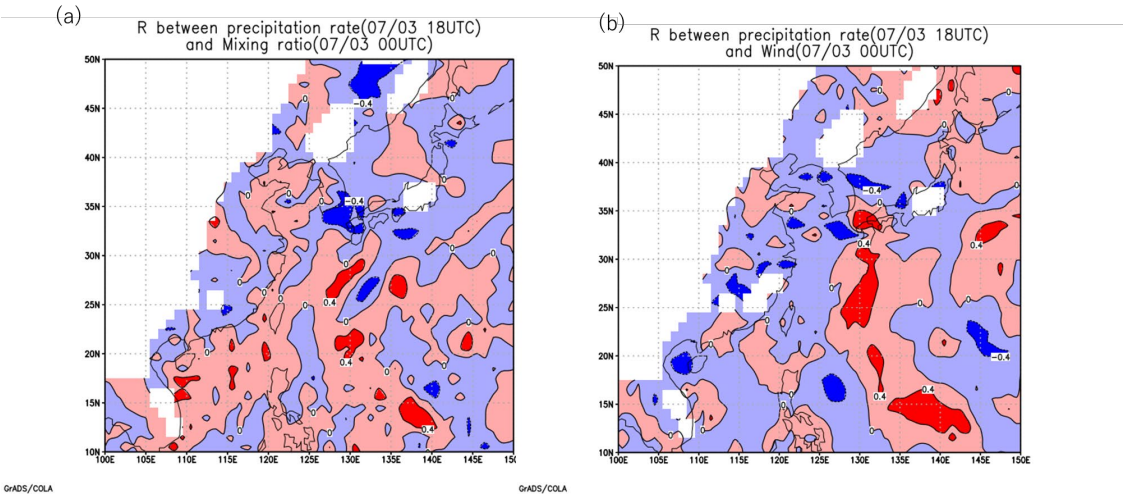

Fig. 7: Horizontal distributions of the correlation between (a) precipitation rate at 18:00 UTC on 3 July and water vapor at 00:00 UTC on 3 July and (b) precipitation rate at 18:00 UTC on 3 July and wind speed at 00:00 UTC on 3 July.

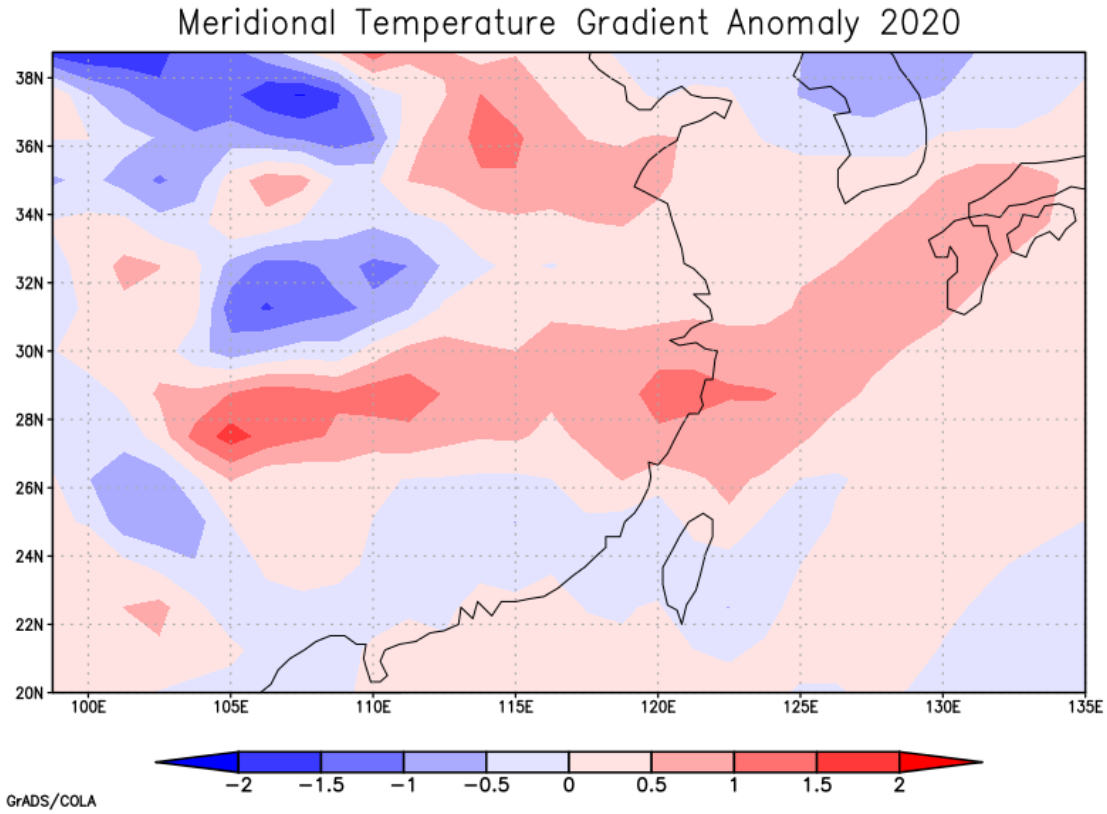

Fig. S1: Horizontal distribution of the anomaly of the meridional temperature gradient [K 2.5°] on the 1000-hPa surface in 2020 relative to the 20-year average.

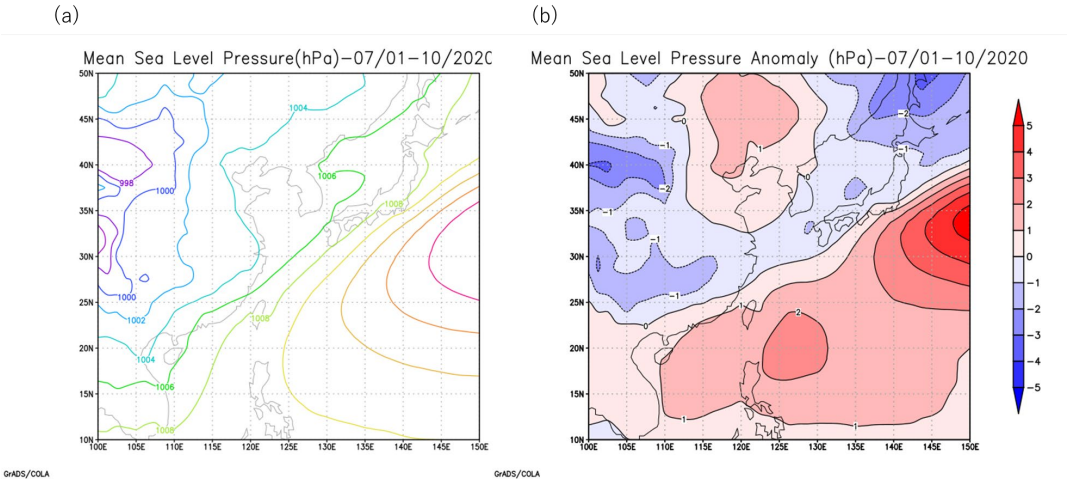

Fig. S2: Horizontal distribution of (a) the sea level pressure [hPa] averaged over the period from 1 to 10 July 2020 and (b) its anomaly relative to the 20-year average over the same period.